# *Supporting Information*

## Study of MDM2 Binding to p53-Analogues: Affinity, Helicity and Applicability to Drug-Design

Ori Kalid* and Nir Ben-Tal

*Department of Biochemistry, George S. Wise Faculty of Life Sciences, Tel-Aviv University, Ramat Aviv 69978, Israel*

## Table of Contents

# Evolution of the simulation protocol

## CHARMM implicit-solvent MM-GB/SA

Simulations were performed with standalone CHARMM[1] using the GB/SW implicit solvent model. System equilibration was monitored by measuring backbone RMSD and potential energy fluctuations. Initially, the simulation was conducted according to protocol 1 described below (see Simulation Details). Following the equilibration phase, the system remained stable for the duration of the 500ps production phase (Figure S1), with an RMSD of 1.5Å - 2Å from its initial conformation. Despite the apparent stability, visual inspection of the molecular-dynamics trajectory revealed potential unrealistic motions. The Chi1 angle of p53 Phe19 changed from $180^0$ to $80^0$ and less after only 70ps of the equilibration phase, and remained lower than $80^0$ along the entire production phase, effectively being outside the binding grove although still maintaining an aromatic interaction with hMDM2 Tyr67. In comparison, this rotamer has not been sampled in the explicit water dynamics performed by Zhong et al.[2]. However, it is not clear whether this conformation is completely unrealistic or simply reached faster in the implicit-solvent simulation. Therefore, we continued the MM-GB/SA analysis under the assumption that a good correlation between predicted and experimental binding affinities will indicate a physically relevant conformational ensemble. Single-trajectory MM-GB/SA was performed due to the high flexibility of the unbound 15-mer which may lead to inadequate conformational coverage. This method, which extracts the conformational ensemble of the unbound protein/ligand from the ensemble of the protein-ligand complex, has been shown to reach better convergence than the multiple trajectory

approach[3-5] (see Simulation Details). Entropy was estimated with normal mode analysis of the energy minimized complex as suggested by Massova and Kollman[3] as well as quasi-harmonic analysis of the molecular dynamics trajectory (see Simulation Details below). As an initial test, the calculation was performed for five representative p53(15-29) derivatives (p53(15-29), p53(15-29)pS15, p53(15-29)pT18, p53(15-29)Trp23Nal, p53(15-29)Leu26Phe). MM-GB/SA energies were calculated from several overlapping sampling windows. Unfortunately, no correlation was found between predicted and experimental binding affinities, independent of the sampling window, inclusion/exclusion of the entropy term and the type of entropy calculation applied (data not shown). This initial result indicates that the ensemble is of low quality. However, before completely discarding the current simulation, the production phase was extended to 3ns, giving the system the opportunity to better equilibrate. Analysis of the new ensemble showed that the potential energy continues to drop after the first 500ps of production, stabilizing at ~1.2ns around a lower energy value (Figure S2). RMSD remains stable until ~1.6ns, after which the ligand starts to drift away from its initial conformation, completely losing the hydrogen-bond between p53 Trp23 and hMDM2 Ile54 after ~2.0ns of production. Ligand drifting of similar magnitude was also witnessed by Zhong et al. in their explicit water simulations[2] and so cannot be regarded a pure artifact of the implicit solvent simulation. Moreover, in the simulation of Zhong et al. the ligand drifts much faster, starting at ~1ns and gaining maximum drift after ~1.7ns compared to ~1.6ns and 2.6ns in the present simulation, respectively. However, until ligand drifting begins, the explicit solvent simulation remains stable around an RMSD of ~1Å, while the present implicit solvent simulation fluctuates close to 2.0Å, possibly indicating some inherent instability, leading

to a greater divergence from the crystal structure. The window for sampling was determined from the p53(15-29)-hMDM2 simulation as the interval between 1.2ns and 1.6ns and MM-GB/SA energies were calculated. No improvement was observed in the correlation. The conclusion at this point was that the molecular dynamics ensemble was not reliable and several approaches were tested to improve accuracy.

The first thing that came to mind was a potential problem with the simulation protocol. CHARMM dynamics was performed with a combination of the Leapfrog Verlet integrator with simple temperature scaling during equilibration, followed by Berendsen temperature control during production (These parameters are recommended in the Accelrys DStudio2.0[6] as well as in the CHARMM documentation). The conformational change in Phe19 occurring during the equilibration phase may point to inadequate temperature control which can lead to unrealistic forces. Therefore, the simulation protocol was modified, uniting the equilibration and production phases, and replacing both temperature scaling and Berndsen coupling with the more accurate Nose-Hoover temperature control (protocol 2, see Simulation Details below). As a result of this modification, Phe19 remained stable throughout the 500ps simulation compared to merely 70ps of the previous simulation and so did the Trp23 hydrogen bond. This indicates that Nose-Hoover is indeed more robust and should probably be the method of choice. The window for sampling was determined from the p53(15-29) simulation and MM-GB/SA was calculated for the same five representative peptides. However, despite the increased stability there was still no improvement in the correlation.

Following a suggestion by CHARMM developers that Nose-Hoover is more suitable for use with the Velocity Verlet integrator rather than Leapfrog Verlet (personal

communication) and that Nose dynamics should generally not be executed with a prior heatup phase, the simulation was rerun with two different combinations: Nose-VVER following heatup and without prior heatup (protocols 3 and 4, respectively, see Simulation Details below). In the protocol 3 simulation, structural stability over the simulated period was similar to protocol 2, but significantly better correlations with binding affinity were observed ($R^2$=0.59, Figure S3). However, protocol 4, in which there was no heating phase, led to a less stable simulation characterized by significantly larger RMS drifts and MM-GB/SA was not calculated. The optimal combination of parameters for the present implicit solvent simulation system is Nose-Hoover dynamics with VVER integration and a prior gradual heatup stage. This may not be the case for more enclosed systems that are less prone to unrealistic motions caused by the lack of constraining water molecules.

Believing that a better correlation can be obtained, the test was repeated with MacroModel Stochastic Dynamics simulations, which also provide robust temperature control.

## MacroModel implicit-solvent MM-GB/SA

MacroModel Stochastic Dynamics simulations were performed as described in the Experimental Section in the main text. This simulation was more stable energetically but less stable conformationally than the CHARMM Nose-VVER simulation (Figure S4). The interaction with Phe19 remained stable throughout the simulations but the hydrogen-bond with Trp23 was lost after ~460ps. Surprisingly, calculation of MacroModel MM-GB/SA energies over the stable period between 200-400ps resulted in a significantly

better correlation with experimental pKd values than the best CHARMM correlation ($R^2$=0.75 vs $R^2$=0.5, Figure S5). In addition, MacroModel GB/SA simulations are 2-fold faster than the CHARMM GB/SW simulations, taking ~0.5hr per 10ps compared to ~1hr, respectively, on a single CPU (Intel Xeon E5310 1.60GHz, 2GB RAM). Therefore, the analysis reported in this paper was carried out in MacroModel, focusing on the simulation period before extensive (and potentially unrealistic) conformational sampling begins.

## MM-GB/SA for peptides terminating at Leu26 and peptidomimetics

Both p53 analogues terminating at Leu26 and peptidomimetic inhibitors were initially modeled in complex with the MDM2 structure from 1YCR (Methods). p53(18-26) and p53(19-26) were excluded from the analysis since the removal of Glu17 leads to a loss in binding energy that is probably an artifact, as discussed above. For the remaining four p53 analogues, a significant negative correlation with $R^2$=0.66 was obtained. This is unanticipated given the significant positive correlations obtained for the p53(15-29) analogues. No correlation was obtained for the peptidomimetics,

A possible reason for this inconsistency is the limited conformational coverage of the current MD simulations resulting from the limited simulation time-scale prior to ligand drifting, and consequent dependence on initial conformation. The contrast between success for long peptides and complete lack of correlation for short peptides and peptidomimetics may indicate that p53 analogues of different sizes bind distinct conformations of MDM2 and that the conformation required for binding short peptides and mimetics was not obtained by MD starting at the 1YCR conformation. Size-dependent induced-fit effects in MDM2 have previously been proposed by Schon et al.,

who described distinct chemical shifts in MDM2 in response to peptides of different lengths[7]. The most distinctive feature of MDM2 in 1YCR compared with MDM2 in 1T4F and co-crystal structures with small molecules (1RV1, 1T4E) and peptidomimetics (2AXI, 2GV2), is the side-chain conformation of Tyr100. In 1YCR, the chi-1 angle of Tyr100 is in *trans* conformation while in the other structures it is in *gauche(-)*. Thus, we manually modified the side-chain conformation of Tyr100 (using Maestro adjust-rotamer tool[8]) and repeated the calculation. A limited improvement was observed in the rank ordering of peptidomimetic compoudns ($R^2$ =0.6 for the 8-mers and $R^2$=0.5 for the beta-hairpins) and no improvement was obtained for the short peptides. Consequently, we repeated the calculation using the structure of MDM2 from 1T4F, a structure adjusted for binding a 9-mer analogue of p53(18-26).

For the short peptides, an improved correlation was obtained ($R^2$=0.44), which could be further enhanced by removing p53(17-26)Phe19MePhe. Analysis of the MD trajectory of this peptide revealed that the conformational fluctuations of the bound peptide during MD were much larger than for the rest of the peptides, suggesting a poor starting conformation and inadequate sampling. For the remaining three peptides 1T4F-based MM-GB/SA yielded a correlation with $R^2$=0.9, while a negative correlation with $R^2$=0.8 was obtained for the same set with 1YCR-based calculations, which completely missed the effect of the Trp23Nal mutation.

For the peptidomimetic inhibitors, the results have also greatly improved: $R^2$=0.86 for 8-mer mimetics (Figure 9a in main text); $R^2$=0.93 for the beta-hairpins; $R^2$=0.89 for the beta-hairpins combined with p53 analogues (Figure 9b in main text).

These results imply that Tyr100 may not be the only structural feature distinguishing the conformation of MDM2 bound to p53(15-29) from its conformations bound to smaller peptides and mimetics. Looking for distinguishing features, we superimposed MDM2 structures from 1YCR, 1T4F, 2AXI, 2GV2, 1RV1 and 1T4E (representing conformations adjusted for binding p53(15-29), peptides terminating at Leu26, peptidomimetics and small molecule inhibitors) and calculated the pair-wise backbone and all-atom RMS deviations. Both superimposition and RMS calculations were done in DiscoveryStudio[6]. The structural diversity found among structures adapted for binding shorter peptides and mimetics was similar to their deviation from the 1YCR conformation. Thus, while 1T4F is clearly a better template than 1YCR for MM-GB/SA of peptides terminating at Leu26 and their analogues, the reasons beyond the conformation of Tyr100 remain unclear at this point.

Interestingly, while good correlations were obtained separately for long peptides and for short peptides and peptidomimetics, the two regression lines are shifted vertically and the correlation is lost when combining the sets. The lower energies are predicted for the p53(15-29) analogues. It would seem that factors that are missing in the current calculation are involved. As discussed in the Introduction section of the main text, one such factor may be the displacement of the N-terminal binding-site lid by peptides stretching beyond Leu26, potentially disfavoring the binding of p53(15-29) analogues. While entropy may also bias against the binding of longer peptides, the magnitude of the entropic effect may be limited. The short peptides considered here differ from their

longer versions in lacking residues 15 and 16 and terminating at position 26. Since residues 15 and 16 extend into solvent and were too mobile to be resolved in the crystal structure, no entropy loss is predicted for these residues upon binding. Residues 28 and 29 do interact with MDM2 but still preserve some of their flexibility, being partially disordered in the crystal[9]. This implies that the major entropy loss upon binding is associated with the helical region of the peptide which is common to both long and short p53 analogues. Another potential biasing factor is the contribution of Glu28 and Asn29 to the binding energy of p53(15-29) analogues, which is probably overestimated by the calculation, as discussed in the main text.

## CHARMM Simulation Details

Molecular-dynamics protocol 1: Complexes prepared using the procedure described above were typed using the CHARMM Momany and Rone force-field[6]. Solvent effects were modeled with the GB/SW implicit-solvent model. Structures were energy minimized using the Steepest-Descent algorithm followed by Adopted-Basis Newton-Raphson, both terminating after 2000 steps or after reaching a gradient of 0.01kcal/mol. The following molecular dynamics cascade was then carried out with command-line CHARMM c33b1: Gradual heatup from 50K to 300K over a period of 20ps with 5K increments at 400ps intervals; Equilibration for 200ps at constant temperature; 500ps production phase at constant temperature was later extended to 3ns. All bonds to hydrogen atoms were constrained using the SHAKE algorithm, allowing a timestep of 2fs, the Leapfrog Verlet integrator was used and temperature control was obtained with the Berendsen algorithm. Coordinates were saved at 2ps intervals.

Molecular-dynamics protocol 2: Same as protocol 1, except for: Nose-Hoover temperature control instead of the Berndsen method, 500ps equilibration+production.

Molecular-dynamics protocol 3: Same as protocol 2, but with the Velocity-Verlet integrator instead of Leapfrog-Verlet.

Molecular-dynamics protocol 4: Same as protocol 3, but with extended equilibration instead of a heatup phase.

In preparation for single-trajectory MM-GB/SA, separate trajectories for the protein and the ligand were extracted from the trajectory of the complex. MM-GB/SA calculations were performed using a combination of perl and CHARMM scripts. Entropy was estimated using VIBRAN module of CHARMM. The quasiharmonic approximation was applied to the sampled frames using the QUASI command. The harmonic approximation was applied to the initial minimized structure using DIAG ENTRopy. In CHARMM, normal-mode calculation requires minimization to a gradient of 10^-6 and cannot be performed with an implicit-solvent model. Therefore, prior to normal mode calculation a distance-dependent dielectric of 4.0 of applied instead of the GB/SW solvent model and the structures were further minimized until the required gradient was reached.

# Figures

## Figure S1

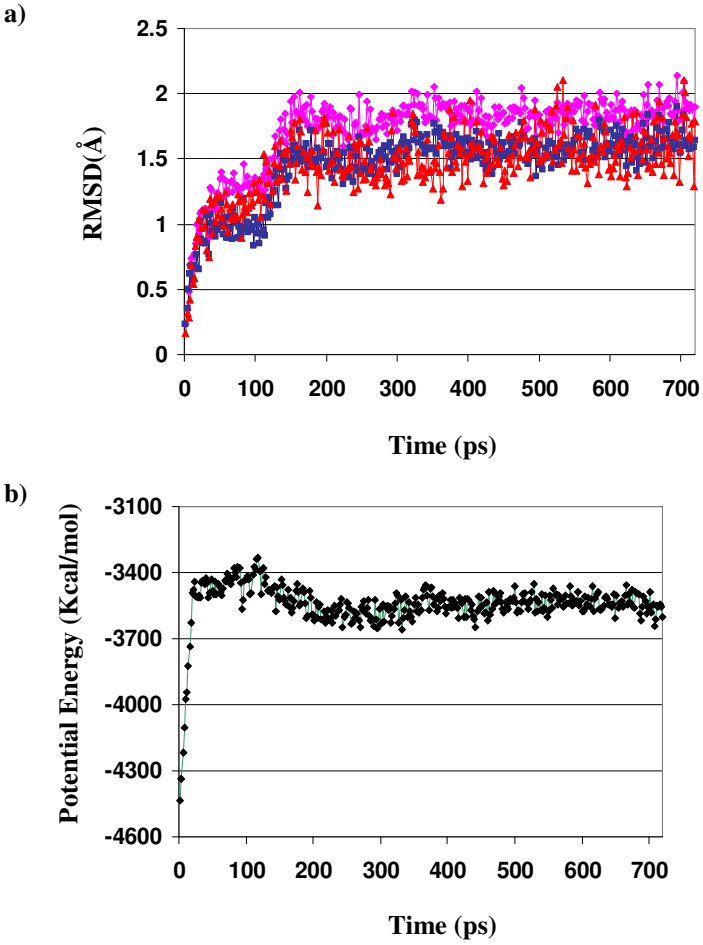


**Figure S1.** CHARMM simulation of hMDM2-p53(15-29) complex, protocol 1. Simulation length is 740ps including 20ps heatup, 200ps equilibration and 500ps production. Frames were sampled every 2ps. **a)** Backbone RMSD deviation relative to the initial structure. Magenta: complex, Blue: protein alone, Red: ligand alone. Ligand RMSD calculation does not include p53(15-16). These residues were disordered in the crystal structure and are expected to fluctuate considerably. Following equilibration the

complex stabilizes between 1.5Å and 2Å from its initial conformation. **b)**. Energy fluctuation. Following equilibration, the system stabilizes around -3600kcal/mol.

**Figure S2**

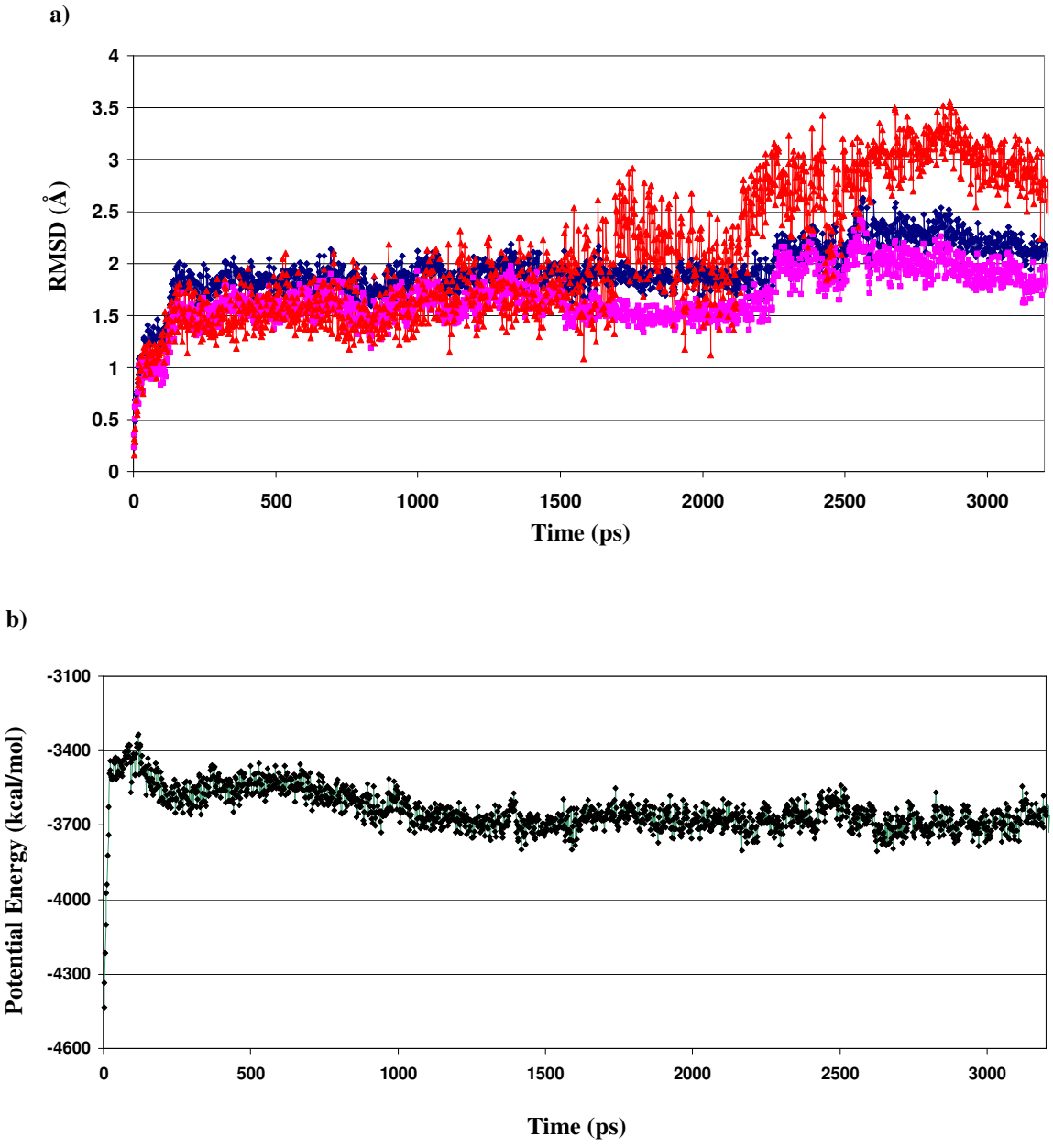


**Figure S2.** CHARMM simulation of the hMDM2-p53(15-29) complex, protocol 1. Simulation length is 3220ps, including 20ps heatup, 200ps initial equilibration and 3ns

production. Frames were sampled every 2ps. **a)** Backbone RMSD deviation relative to the initial structure. Magenta: complex, Blue: protein alone, Red: ligand alone. Ligand RMSD calculation does not include p53(15-16). These residues were disordered in the crystal structure and are expected to fluctuate considerably. After heatup and initial equilibration the complex remains stable around 2.0Å from its initial conformation until ~2.1ns of production. However, the ligand starts to sample conformations after about 1.4ns of production and gains larger RMSD deviations as the simulation proceeds. **b)** Energy fluctuation. After roughly 1ns of production the system stabilizes around -3700kcal/mol. Between 1ns and 1.4ns the system is stable both in terms of energy and backbone RMSD fluctuations.

**Figure S3**

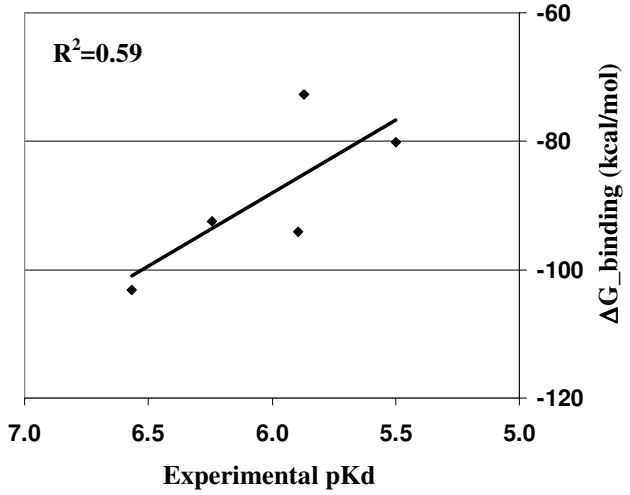


**Figure S3. C**orrelation between CHARMM MM-GB/SA energies and experimental pKd values for a representative set of five p53(15-29) derivatives, calculated with simulation protocol 3. The observed correlation is better than with protocol 2, showing the

sensitivity of the method to the choice of integrator as well as temperature-control algorithm.

**Figure S4**

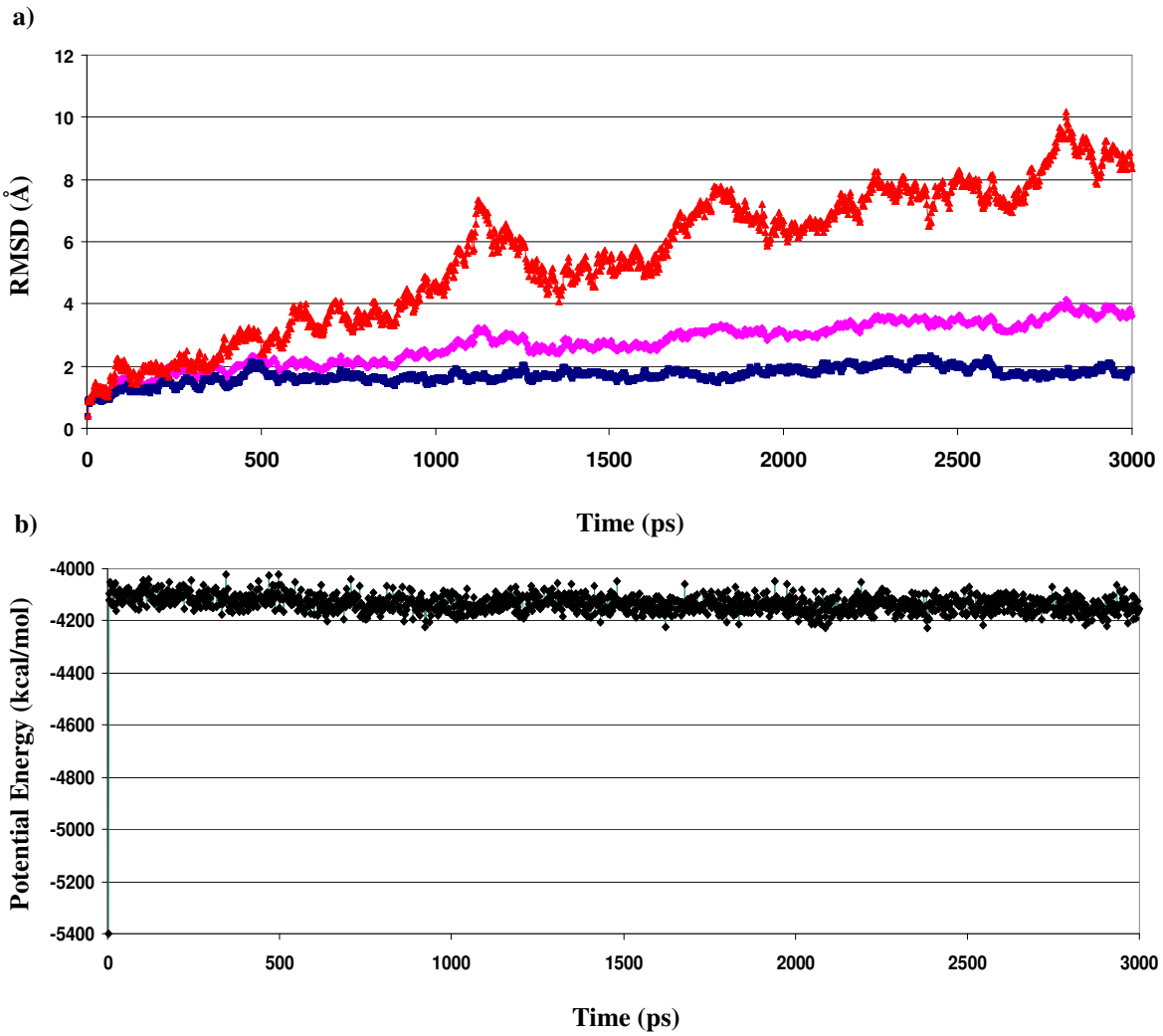


**Figure S4.** MacroModel simulation of the hMDM2-p53(15-29) complex. **a)** backbone RMS deviation relative to the initial structure. Magenta: complex, Blue: protein alone, Red: ligand alone. Ligand RMSD calculation does not include p53(15-16). These residues were disordered in the crystal structure and are expected to fluctuate considerably. The protein remains stable around 2Å from its initial conformation. The ligand starts drifting after ~200ps and reaches much larger RMSD deviations than in the

CHARMM simulations. **b)** Energy fluctuation. The system stabilizes quickly around -4100kcal/mol.

**Figure S5**

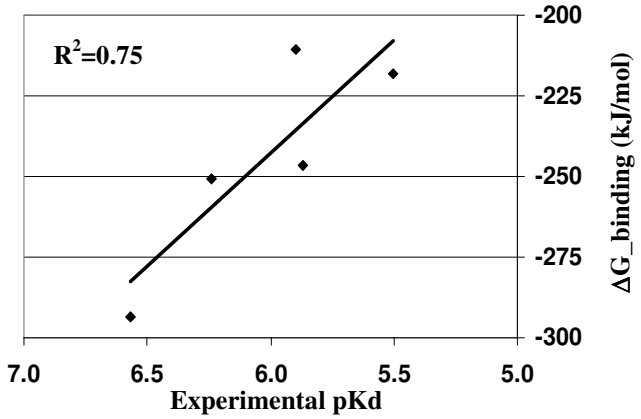


**Figure S5**. Correlation of MacroModel MM-GB/SA energies with experimental pKd values for a representative set of five p53(15-29) derivatives. A good correlation was observed, with $R^2$=0.75, much better than that achieved with the corresponding CHARMM simulations.

# References


1. *CHARMM*, Version C33b1; Accelrys, Inc.: San Diego, CA, 2008.
2. Zhong, H.; Carlson, H. A. Computational studies and peptidomimetic design for the human p53-MDM2 complex. *Proteins* **2005,** *58*, 222-234.
3. Massova, I.; Kollman, P. A. Computational Alanine Scanning To Probe Protein-Protein Interactions: A Novel Approach To Evaluate Binding Free Energies. *J. Am. Chem. Soc.* **1999,** *121*, 8133-8143.

4. Lee, H. J.; Srinivasan, D.; Coomber, D.; Lane, D. P.; Verma, C. S. Modulation of the p53-MDM2 interaction by phosphorylation of Thr18: a computational study. *Cell cycle (Georgetown, Tex* **2007,** *6*, 2604-2611.

5. Gilson, M. K.; Zhou, H. X. Calculation of protein-ligand binding affinities. *Annu. Rev. Biophys. Biomol. Struct.* **2007,** *36*, 21-42.

6. *Discovery Studio*, Version 2.0; Accelrys, Inc.: San Diego, CA, 2008.

7. Schon, O.; Friedler, A.; Freund, S.; Fersht, A. R. Binding of p53-derived ligands to MDM2 induces a variety of long range conformational changes. *J. Mol. Biol.* **2004,** *336*, 197-202.

8. *Maestro*, Version 8.0; Schrodinger, LLC: New York, NY, 2005.

9. Kussie, P. H.; Gorina, S.; Marechal, V.; Elenbaas, B.; Moreau, J.; Levine, A. J.; Pavletich, N. P. Structure of the MDM2 oncoprotein bound to the p53 tumor suppressor transactivation domain. *Science* **1996,** *274*, 948-953.